ISIJ International, Vol. 44 (2004), No. 3, pp. 492–499

Modeling of Combustion and Heat Transfer in an Iron Ore Sintering Bed with Considerations of Multiple Solid Phases

Won YANG, Changkook RYU, Sangmin CHOI, Eungsoo CHOI,[1)] Deokwon LEE[1)] and Wanwook HUH[1)]

Department of Mechanical Engineering, Korea Advanced Institute of Science and Technology, Guseong-dong, Yuseong-gu, Daejeon, 305-701, Korea. E-mail: smchoi@kaist.ac.kr 1) POSCO, Tech. Res. Labs., Goedong-dong, Nam-gu, Pohang, Gyeongbuk, 790-785, P.O. Box 36, Korea.

(*Received on August 11, 2003; accepted in final form on October 9, 2003*)

The iron ore sintering was characterized as a relatively uniform process of solid material, coke combustion, various modes of heat transfer, and the complicated physical changes of solid particles. The sintering bed was modeled as an unsteady one-dimensional process of the solid materials with multiple solid phases, which confers a phase on each kind of solid material. Each solid phase had a specific particle size and compositions. Drying, condensation, coke combustion, limestone decomposition, generation of the macroscopic internal pore and shrinking of the bed were considered. Complicated modes of heat transfer including conduction, convection and radiation were considered. Numerical simulations of the condition in the iron ore sintering bed were carried out for various parameters: coke contents and air suction rates, along with some other parameters of the model. Calculation results were compared with the results of the sintering pot test. The temperature profiles and gas compositions showed a good agreement with the experimental data.

KEY WORDS: iron ore sintering; mathematical model; multiple solid phase; coke combustion; heat transfer.

1. Introduction

The iron ore sintering process is applied to produce large particles (>∼5 mm) of iron ore agglomerates with appropriate metallurgical properties required in the blast furnace. A raw mix of iron ores, limestones, and fuel coke fines forms a bed on a traveling grate. **Figure 1** shows a conceptual version of the process in the iron ore sintering bed. Once ignited by a coke oven gas (COG) burner, coke combustion progresses downward very slowly, and iron ores are sintered in the high temperature (combustion) zone. Air is supplied to the bed by a down draft suction fan. The combustion commences at the top of the bed by a hot gas jet from the ignition burners for a few minutes after the feed material is introduced into the bed, and propagates into the bed with sintering near the combustion front.

An iron ore sintering bed is relatively homogeneous and static compared with waste incinerators of grate type. That makes it easier to model it as a fixed bed which moves at constant speed. Many researchers conducted modeling coke combustion and heat transfer in the iron ore sintering bed. Muchi and Higuchi[1)] performed one dimensional modeling of the sintering bed focused on the coke combustion and predicted combustion gas composition and temperature distribution in the bed. Young[2)] considered the change of coke particle size during combustion in addition to the bed combustion model. Cumming *et al*.[3)] and Patisson *et al*.[4)] considered the change of the bed height and porosity that resulted from the surface melting of the iron ore by introduction of shrinkage factor. Nath *et al*.[5)] predicted the melting and molten zone in addition to the previous model. Kasai *et al*.[6)] employed the discrete element method (DEM) and analyzed bed structural changes systematically, and Ramos *et al*.[7)] combined this method with the combustion and heat transfer modeling in the iron ore sintering bed. But there is still enough potential for the improvement of the models in point of solid fuel combustion and heat transfer in porous media, although they well describe the complicated phenomena in the sintering bed. First of all, these models are one-dimensional and consider the solid part as a single phase that has a uniform chemical composition. Each cell is represented by unique solid temperature, chemical composition and physical properties. These representations can be somewhat different from the real situation, in which each kind of solid material has different temperatures, physical properties and chemical compositions. Secondly, heat transfer in the sintering bed should be treated in detail in order to understand the influence of various design and operating parameters on the conditions in the bed. Especially radia-

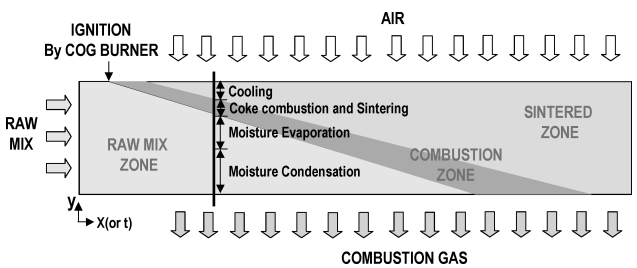

Fig. 1. Schematic diagram of the iron ore sintering process.

tion, which has not been considered in the previous studies, can be one of the important phenomena for describing the propagation of the combustion zone in porous media.[8] Finally, modeling of the geometrical changes in the solid particles and whole sintering bed can be performed in a new manner for improving applicability to a different type of fixed/moving beds involving solid fuel combustion.

Starting with a consideration of multiple solid phases and various modes of the heat transfer in detail can be the first step in solving these problems and improving the mathematical model of an iron ore sintering bed. In this research, simulations of the iron ore sintering process with the consideration of the multiple solid phases have been developed with employing the series of conservation equations for each phase. Mathematical equations of coke combustion, limestone decomposition, and various modes of heat transfer in/between identical/different solid phases which include radiation as well as convection and conduction were developed for calculating source terms of the conservation equations. New method of the modeling geometrical changes of the solid particles and the sintering bed has been proposed. Simulation results were compared with the results of sintering pot test.

2. Model Outlines and Governing Equations

Figure 2 shows the concept of the process modeling with multiple solid phases. The sintering bed consists of a gas phase and multiple solid phases including iron ores, coke, limestone and other minor additives. The mix of the solid phases can be considered as porous media. Each solid phase has a different particle size and chemical composition. When heated by hot gas stream generated by a gas burner, solid material experiences drying, coke reactions, limestone decompositions, or reduction of the iron oxide. For large particles, multiple kinds of reactions can occur in a single particle due to the temperature gradient. Through these processes, heat and mass exchange between solid and gas occur.

Geometrical change is also an important parameter in the model. Changes of the particle sizes during combustion, melting, or sintering cause a change of bed structure, which can be represented by bed height and porosity. Generation of internal pores during drying or coke combustion changes the particle densities and other physical properties, which should be modeled carefully because they can significantly influence on the combustion process and quality of the sintered ore.

Mathematical modeling of these phenomena is composed of constructing system equations of conservation form based on the assumption that the solid and gas are continuum. Sub-models are required to determine each term of the governing equations. **Table 1** shows the meaning of the

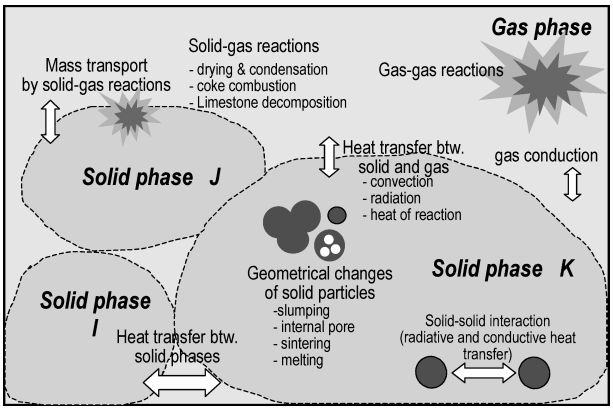

Fig. 2. Major phenomena in the sintering bed.

Table 1. Symbols used in this paper.

Symbol	Unit	Meaning	Symbol	Unit	Meaning
A_s	M^2/m^3	Volumetric surface area	T	K	Temperature
A_r	M/s-K	Frequency function	T_{m1}	K	Initiation temperature of melting
C	$kmol/m^3$	Molar concentration	T_{m2}	K	Completion temperature of melting
Cp	J/kg-K	Specific heat	t	sec	Time
D	m^2/s	Gas diffusivity	W	kg/kmol	Molecular weight
d_p	m	Particle diameter	v	m/s	Velocity
d_r	m	Real diameter	y	m	Coordinate along the height
d_u	m	Diameter of the unreacted part	y		Fraction of heat absorbed by solid
d_o	m	Initial diameter			
E_r		Activation energy	**Greeks**		
F	-	Mass of coke/Initial mass of coke	ρ	kg/m^3	Density
f_{AS}	-	Fraction of the ash segregated	ε		Bed porosity
fs	-	Shrink factor	ε_{ip}		Fraction of internal pore
f_V	-	Volume fraction	ζ		Particle area factor
FFS	cm/min	Flame front speed	κ		Absorption coefficient
h	J/kg	Enthalpy/Unit mass	ν		Stoichiometric coefficient
h_{conv}	W/m^2-K	Convective heat transfer coefficient	τ		Optical thickness
I	W/m^2sr	Radiation intensity	ω		Single scattering albedo
ΔH_r	J/kg-s	Reaction heat			
K		Equilibrium constant	**Subscripts**		
k	W/m-K	Thermal conductivity	comb		Combustion
k_r	m/s	Rate coefficient (Arrhenius form)	g		Gas
k_m	m/s	Gas film mass transfer coefficient	i		Index of coke reactions
k_{eff}	m/s	Mass transfer coefficient (ash layer)	j		Cell number
M_f	-	Melt fraction	I, J		Index of solid phase
M	kg/m^3s	Volumetric mass generation rate	k		Solid or gas component
m		Mass fraction	l		Limestone
n		Packing parameter	r		Index of the reaction
n_p	$/m^3$	Particle number density	rad		Radiation
p	Pa	Pressure	r_s		Solid-gas reactions
q	J/kg-s	Volumetric heat generation rate	s		Solid
R	KJ/kg-K	Universal gas constant			

Table 2. Governing equations.

Solid phases (for phase I)	Mass	$\frac{\partial(\rho_{s,I}f_{V,I})}{\partial t}+\frac{\partial(\rho_{s,I}v_{s,I})}{\partial y}=\sum_{\substack{phase\,J\\ I\neq J}}\dot{M}_{solid-gas\ reactions,I\to J}$	(3)
	Energy	$\frac{\partial(f_{V,s,I}h_{s,I})}{\partial t}+\frac{\partial v_{s,I}h_{s,I}}{\partial y}=\frac{\partial}{\partial y}\left(f_{V,s,I}k_{s,I}\frac{\partial T_{s,I}}{\partial y}\right)+\sum_J h_{JI}A_{s,I}(T_{s,J}-T_{s,I})+\sum_l h_{conv,g-I}A_{s,I}(T_g-T_{s,I})+\frac{f_{v,I}}{1-\varepsilon}q_{rad}+\sum_{r_s}y_I\dot{M}_{s,I,r_s}\Delta H_r-\left(\sum_{r_s}\dot{M}_{s,I,r_s}\right)C_{p,I}T_{s,I}$ where $A_{s,I}=n_{p,I}A_{p,I}$: volumetric surface area of the particles [m^{-1}]	(4)
	Compo-nents	$\frac{\partial(\rho_{s,I}f_{V,I}m_{s,I,k})}{\partial t}+\frac{\partial(\rho_{s,I}v_{s,I}m_{s,I,k})}{\partial y}=\sum_{r_s}\dot{M}_{s,I,k,r_s}$	(5)
Gas phase	Mass	$\frac{\partial\rho_g\varepsilon}{\partial t}+\frac{\partial\rho_g v_g}{\partial y}=-\sum_I\sum_{r_s}\dot{M}_{s,I,r_s}$	(6)
	Energy	$\frac{\partial(\varepsilon h_g)}{\partial t}+\frac{\partial(v_g h_g)}{\partial y}=\frac{\partial}{\partial y}\left(\varepsilon k_g\frac{\partial T_g}{\partial y}\right)+\sum_l h_{conv,g-I}A_{s,I}(T_{s,I}-T_g)+\sum_{r_s}(1-y_I)\dot{M}_{s,I,r_s}\Delta H_{r_s}+\left(\sum_{r_s}\dot{M}_{s,I,r_s}\right)C_{p,I}T_{s,I}$	(7)
	Chemical species	$\frac{\partial(\rho_g\varepsilon m_{g,k})}{\partial t}+\frac{\partial(\rho_g v_g m_{g,k})}{\partial y}=\sum_{r_s}\sum_I\dot{M}_{s,I,k,r_s}+\sum_{r_g}\dot{M}_{g,k,r_g}$	(8)
	Equation of state	$\rho_g=p/R\sum\frac{m_j}{W_j}T_g$	(9)

symbols used in this paper.

Governing equations have a form of unsteady and one-dimensional partial differential equations. Unsteady terms of the equations can be transformed to the location along the direction of the moving grate, which progresses with constant speed. Velocity v is a superficial velocity based on the assumption of the plug flow. Volume fractions of each phase are reflected in the generalized form of the transport equation of scalar quantity ϕ.

Solid phases, for solid phase I,

$$\frac{\partial(\rho_{s,I}f_{V,s,I}\phi_{s,I})}{\partial t}+\frac{\partial(\rho_{s,I}v_{s,I}\phi_{s,I})}{\partial y}=\frac{\partial}{\partial y}\left[f_{V,s,I}\Gamma_{s,I}\frac{\partial\phi_{s,I}}{\partial y}\right]+S_{\phi_{s,I}} \quad \text{.....(1)}$$

Gas phase,

$$\frac{\partial(\rho_g\varepsilon\phi_g)}{\partial t}+\frac{\partial(\rho_g v_g\phi_g)}{\partial y}=\frac{\partial}{\partial y}\left[\varepsilon\Gamma_g\frac{\partial\phi_g}{\partial y}\right]+S_{\phi_g} \quad \text{.....(2)}$$

Solid phases and the gas phase influence each other through the pressure difference by packing as well as heat and mass transfer. These effects are reflected in the source terms of the equations. **Table 2** shows the detailed governing equations for each phase. The terms in the right hand side of Eq. (4) mean followings in sequence; diffusion term including conduction, heat transfer from other solid phases, convective heat transfer from gas phase, radiation, heat of various reactions, and heat loss by release of gas produced by reactions.

3. Sub-models

Sub-models determine each term of the governing equations. They consider chemical reactions, various modes of heat transfer and geometrical changes of the solid particles.

3.1. Reactions

Chemical reactions in the sintering bed consist of two parts: solid–gas and gaseous reactions. Major solid–gas reactions in an iron ore sintering bed are coke combustion and limestone decomposition. Generally, the combustion process of solid fuel can be classified into drying, pyrolysis and coke reactions; however, pyrolysis is not considered here because the volatile content in coke is very low. Gas species participate in these reactions as reactant or product. In this point of view, drying and moisture condensations also can be regarded as solid–gas reactions.

Coke reactions occur in the surface of the solid particle. O_2, CO_2, H_2 and water vapor can participate in the reactions as a reactant competitively. These reactions are heterogeneous and can be classified as the oxidation and gasification. Temperature, gas diffusion and change of the particle sizes are important parameters in the coke reactions, which are expressed as a form of the rate equation, Eq. (10).

$$R_i^{o,g}=\frac{A_s v_s W_{char}C_{g,i}d_p}{\frac{1}{k_r\zeta}+\frac{1}{k_m}+\frac{1}{k_{eff}}} \quad \text{.....(10)}$$

where

$$A_s=(\pi d_p^2)\frac{6f_{V,I}}{\pi d_p^3},\quad k_r=A_rT\exp\left(-\frac{E_r}{RT}\right),$$

$$\frac{1}{k_{eff}}=\frac{(1-F)d_p}{2D_{eff}}$$

Another important solid–gas reaction is the limestone decomposition. Young's model[2] can be employed for the prediction of the decomposition rate. Changes of the particle size can be considered in the same way as coke reactions because the reaction is also a kind of surface reaction. Young's model can be described as Eq. (11).

$$R_l = \frac{n_l \pi d_l (C^*_{CO_2} - C_{CO_2})}{\frac{1}{k_m} + \frac{d_p(d_p - d_l)}{d_l D_s} + \frac{2K_l \cdot 4.1868}{k_l R T_s}\left(\frac{d_p}{d_l}\right)} \quad \text{.....(11)}$$

where

$$C^*_{CO_2} = \frac{K_l}{RT_s}, \quad K_l = \exp\left(7.35 - \frac{5211}{T_s}\right),$$

$$k_l\ (\mathrm{kg/m^2\,s}) = 1337.6 \exp\left(-\frac{20143.4}{T_s}\right)$$

As for the gaseous reactions, combustion of the carbon has been considered. The adopted reaction kinetics of CO is expressed as Eq. (12),

$$\frac{dC_{CO}}{dt} = 1.3 \times 10^{11} C_{CO} C^{0.5}_{H_2O} C^{0.5}_{O_2} \exp\left(-\frac{15105}{T_g}\right) \quad \text{.....(12)}$$

Gaseous combustion occurs much faster than solid–gas reactions. In this model, we assumed that gaseous reactant was consumed preferentially for gaseous reactions. Only excessive reactants can participate in the solid–gas reactions.

3.2. Heat Transfer

Heat transfer in the iron ore sintering bed contains very complicated modes of conduction, convection and radiation. It can be summarized as follows: convection/radiation between gas and solid phases, conduction/radiation between solid phases, conduction/radiation between the solid particles (in the same solid phases) and conduction in the gas phase. One solid particle is assumed to have one representative value of temperature, which means that there is no temperature gradient in a single particle.

Wakao and Kaguei[9]'s equation is employed for estimation of the convective heat transfer coefficient between solid phases and gas phase.

$$Nu = 2 + 1.1 Re^{0.6} Pr^{1/3} \quad \text{.....(13)}$$

The two-flux model, suggested by Shin and Choi,[8] was employed for radiative heat transfer between the solid particles of the same phase. This model is a simplified form of the discrete ordinate method, neglecting scattering term. Radiative heat transfer can be obtained by Eqs. (14) and (15). This approximation has the limitation that the actual bed material is not arranged so ideally as shown in **Fig. 3**. However, compared to using radiative conductivity, which is used widely in porous heat transfer studies, this model is further realistic and stable for the calculation procedure.[8]

$$q_{rad} = \pi(I^+ - I^-) \quad [\mathrm{W/m^2}] \quad \text{.....(14)}$$

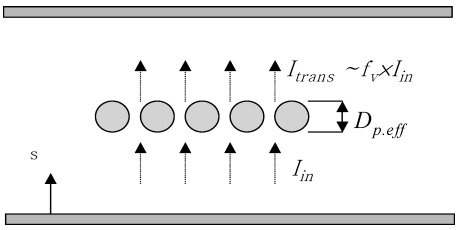

Fig. 3. Radiation absorption to the bed particle.[8]

$$\frac{1}{2}\frac{dI^+}{d\tau} = (1-\omega)I_b - I^+ + \frac{\omega}{2}(I^- + I^+)$$
$$\frac{1}{2}\frac{dI^-}{d\tau} = (1-\omega)I_b - I^- + \frac{\omega}{2}(I^- + I^+) \quad \text{.....(15)}$$

where

$$\tau = \int_0^y (\kappa + \omega)\,dy, \quad \kappa = -\sigma_S - \frac{1}{s}\ln\left(\frac{I_{trans}}{I_{in}}\right) = -\frac{1}{D_p}\ln(f_v)$$

Estimation of heat exchange between solid phases is very difficult due to its complexity. In this study, a form of the convection heat transfer coefficient is used that has been also employed for the estimation of the heat transfer between fluidization particles and wall.[10] Austin *et al.*[11] used this method for the estimation of the heat transfer between iron ore and coke in a blast furnace. Heat transferred from the solid phase J to the solid phase I can be expressed as Eq. (16).

$$q_{ss,IJ} = h_{IJ} A_{s,I} (T_{s,J} - T_{s,I}) \quad \text{.....(16)}$$

where

$$h_{IJ} = \left[\frac{2}{\sqrt{\pi}}\sqrt{\frac{\sum_I f_{V,I}\, k_{s,I} (\rho_s C_{ps})_I + \varepsilon k_g \rho_g C_{pg}}{\sum_I f_{V,I}\, t_s + \varepsilon t_g}}\right]\frac{f_{V,J}}{f_{V,I}}$$

The reciprocity rule should be applied for the heat balance between solid phases, so all the coefficients and surface areas should have a relationship as in Eq. (17).

$$h_{IJ} A_{s,J} = h_{JI} A_{s,I} \quad \text{.....(17)}$$

3.3. Geometrical Changes

All the geometrical changes in the sintering bed are caused by the solid–gas reactions initially. Particle sizes of the coke and limestone are decreased by combustion or decomposition, while sintering can increases particle sizes of the iron ore. These changes cause bed structural changes in areas such as bed height and porosity. Some of the compositions in the solid particles cause a generation of the internal pores during reactions; therefore, modeling geometrical changes in an iron ore sintering process can be categorized into three parts: (1) changes of the particle sizes, (2) generation of the internal pores, and (3) bed structural changes.

In this model, the effects of the iron ore reduction and sintering/melting on the sintering bed are assumed to be negligible. For estimating the effects of coke reactions and limestone decomposition, the behavior of the ash or CaO should be considered. For generalization, f_{AS}, the fraction

segregated from the solid particle is defined by Eq. (18).

$$f_{AS} \equiv \frac{\text{Mass of ash segregated}}{\text{Total mass of ash}} \quad (0 \leq f_{AS} \leq 1) \quad \text{....(18)}$$

Some parameters related to particle sizes should be defined for the determination of the particle size d_p. When d_o is the initial diameter and d_u is the parts containing combustible, d_r, the real particle diameter after segregation, can be obtained from Eq. (19).

$$d_r = [(1-f_{AS})d_o^3 + f_{AS}d_u^3]^{1/3} \quad \text{.....(19)}$$

Through these values, d_p can be obtained by the Eq. (20),

$$d_p = [(1-F)d_u^3 + Fd_r^3]^{1/3} \quad \text{.....(20)}$$

The bed height can be decreased by solid–gas reactions and non-reactive factors such as sintering, melting and shrinkage of the particles. Only reactive-factors are considered in this model. Change of the particle sizes can also change packing methods, significantly affecting the porosity of the bed. Packing parameter n is introduced as Eq. (21) for particle size d_p and shrink factor f_s.[8]

$$f_v = f_s^{1-n} f_v^0 \quad \text{.....(21)}$$

If n is unity, volume fraction remains constant and decreases in particle size cause the bed height to change. If n is zero, the change of the volume fraction causes an increase of the porosity, meaning the bed height does not change.

Another important factor of the geometrical change is the generation of the internal pores, which affect the densities of the solid phases. The decomposition of limestone also affects the generation of the internal pore in the particles. Internal pores are calculated from the form of a partial differential equation expressed as Eq. (22).

$$\frac{\partial f_{V,I}\,\varepsilon_{ip,I}}{\partial t} + \frac{\partial v_s\,\varepsilon_{ip,I}}{\partial y} = -\sum_i f_{ip,i}\frac{\dot{M}_{comb,i}}{\rho_i} + \dot{\varepsilon}_{ip,loss,I} \quad \text{.....(22)}$$

In addition, the surface melting of an iron ore can influence the porosity of the bed. The melt fraction is estimated by Eq. (23).[7] T_{m2} can be obtained from the $CaO–Fe_2O_3$ phase diagram.

$$M_f = \frac{T_{s,ore} - T_{m1}}{T_{m2} - T_{m1}} \quad \text{.....(23)}$$

3.4. Physical Properties

Density, specific heat, thermal conductivity, diffusivity and viscosity of the solid component or gas species should be modeled carefully since they can influence the simulation results directly. They were obtained by summation of the properties of each component multiplied by its mass fraction. The modeling method and references for the calculation of the each solid component or each species are shown in **Table 4**. Chapman–Enskog Theory[12] was employed for estimating gas diffusivity and the Merrick Model[13] was used for setting the properties of coke.

4. Results and Discussion

4.1. Calculation Cases

One of the most important parameters of the sintering process is the coke combustion rate, which is influenced by the coke contents in the material and the air suction rate. Calculation is performed for the various coke contents and air suction rates which are expressed as the initial values of pressure difference after ignition. **Figure 4** shows the iron ore sintering bed simulated in this study.

Table 4 shows the major parameters of the reference calculation case. The three solid phases of iron ore, coke, and

Table 3. Sources of the physical properties of the solid component and gas species.

	Solid component	Gas species
Name	moisture, coke, limestone, iron ore, calcium oxide, inert	O_2, H_2O, CO_2, CO, H_2, N_2
Density	Coke : obtained from the reference[13] Others : obtained from the reference[14]	Obtained from the reference[14]
Specific heat		
Thermal conductivity		
Diffusivity	-	Chapman-Enskog theory[12]
Viscosity	-	Sutherland's law

Table 4. Major input parameters (reference case).

Parameters	Value	Parameters	Value
Mass fractions (%) of		Number of cells	57
Iron ore	83.2	Δy (mm)	10
Coke	3.8	Time step (sec)	1
Limestone	13.0		
Particle diameters (mm) of,		Ignition time (sec)	90
Iron ore	3.2 or 3.0	Gas inlet velocity during ignition (m/s)	4
Coke	1.6	ΔP during ignition (mmAq)	1000
Limestone	1.6	Setting value of ΔP after ignition (mmAq)	1500
Pseudo particle (averaged)	3.0		
Initial internal porosities of,		Packing parameter, n	0.6
Iron ore	0.025	Fraction of reaction heat absorbed by solid, y	
Coke	0.025	Drying	0.9
Limestone	0.025	Coke reactions	0.6
Water contents (%)	7.0	Limestone decomposition	0.7
Porosity of the bed	0.4		

limestone were considered. Other additives, which were not involved in the solid–gas reactions, were considered as parts of the inert material. Each solid phase consists of solid components such as moisture, coke, iron ore, $CaCO_3$, CaO, and inert. Each of them has specific physical properties such as density, specific heat, and thermal conductivity.

Table 5 shows the cases of the calculation and experiment. Main operating parameters are coke contents in the solid material and air inlet velocity, which can be represented by the initial pressure difference. After setting the initial value, the suction pressure varies with the progress of the coke combustion and the sintering of iron ore as shown in **Fig. 5**. Considering these variations, air inlet velocity, which is a function of time, can be considered as the second order polynomial, while pressure difference is not reflected to the calculations. The coefficients are obtained from measurement data of the air velocity.

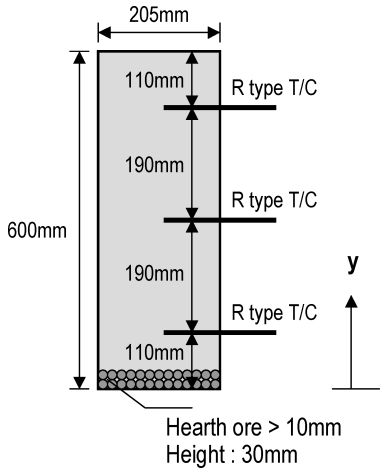

Fig. 4. The sintering bed simulated in this study.

Table 5. Experimental and calculation cases.

Case name	Ini. mass fraction of coke (%)	Air inlet velocity, downward (m/s) $(A + B\bullet t + C\bullet t^2)$			Avg. air velocity (m/s)
		A	B	C	
Coke3.4	3.4	0.350	7.5585×10^{-6}	1.5853×10^{-7}	0.43
Coke3.8	3.8				
Coke4.2	4.2				
AirV0.26	3.8	0.180	-4.653×10^{-6}	1.199×10^{-7}	0.26
AirV0.32		0.230	-4.653×10^{-6}	1.199×10^{-7}	0.32
AirV0.45		0.303	-1.850×10^{-6}	1.747×10^{-7}	0.45
AirV0.52		0.383	-1.850×10^{-6}	1.747×10^{-7}	0.52

4.2. Calculation Results and Discussion

In the pot test, bed height was decreased by approximately 70 mm due to the melting of the iron ore. In the calculation model, in which sintering was not considered, bed height was assumed to have been decreased by coke reactions and limestone decomposition. The decrease of the bed height was tuned by setting the value of the packing parameter. Solid–gas reactions also affected the porosity of the bed, which was to about 0.43–0.44, similar to the selected value from the previous researchers' work.[2)]

Figure 6 shows the simulation results of the temperature distribution in the bed. The increase of the thickness of the coke combustion zone is well simulated. As reported in the previous study,[8)] this unsteady 1-dimensional model can be extended to the 2-D steady model when the time axis is converted to horizontal directions by the constant moving speed.

Simulation data is compared with the pot test data, as represented in **Fig. 7**. Temperatures of the bed at the locations of $y = 0.11$ m, 0.30 m and 0.49 m were measured by R-type thermocouples in the pot test, as is shown in Fig. 4. Figure 7(a) shows the average temperature distribution of the solid phase. Particle diameter and surface area of the each solid material can be reflected to the calculation, and the results are close to the experimental data in maximum temperature, thickness of the combustion zone, and the time of the temperature increase. Figure 7(b) shows the gas compositions of O_2, CO_2 and CO, which are major combustion reactants and products. The values remain constant after ignition and they also show a meaningful agreement

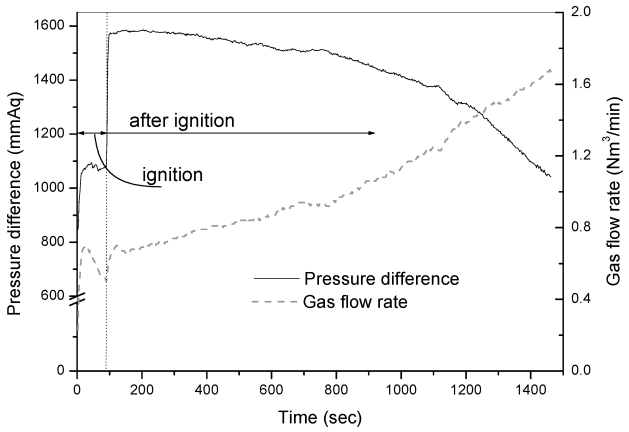

Fig. 5. Typical trends of the pressure difference and gas flow rate in the sintering pot.

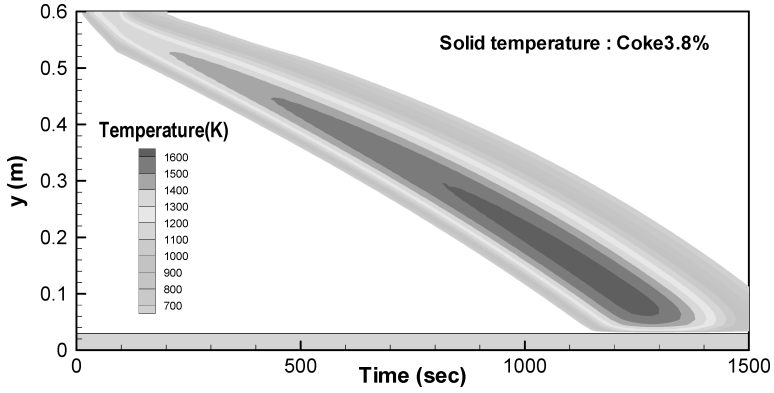

Fig. 6. Simulation results of the temperature distribution in the bed (coke3.8).

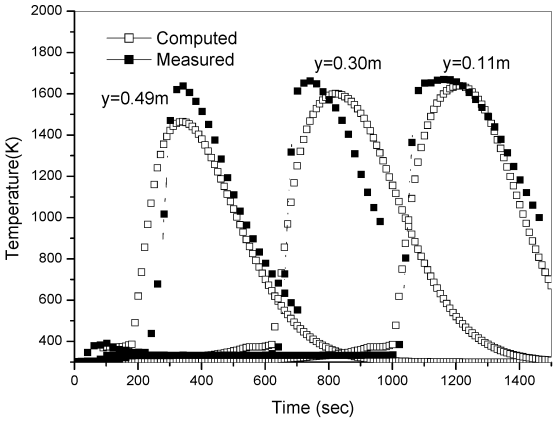

(a) Temperature profiles of solid material

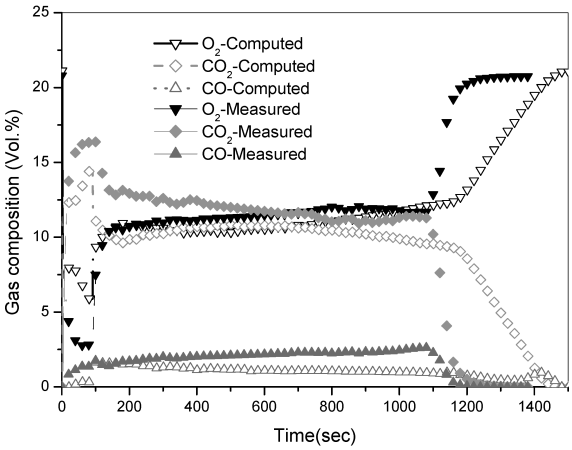

(b) Combustion gas compositions

Fig. 7. Comparison between the measured data and simulation results of coke3.8. (a) Temperature profiles of solid material, (b) combustion gas compositions.

with the experimental data, even if there is a little difference in CO_2 and CO concentrations, which are caused by underestimation of coke combustion rate.

Mass fraction of coke is one of the important parameters that influence the bed temperature and gas composition. **Figure 8** shows the mean solid temperatures at the point of $y=0.30$ m (center of the bed), for various initial mass fractions of coke. Higher coke content in the raw-mix material results in an increase of the combustion zone thickness and maximum temperature, meaning that the melt fraction increases for higher coke content. Simulation results have a similar trend to the experimental results.

In this model, the melt fraction of the iron ore can be estimated based on the mass fraction of CaO in the solid material and temperature of the iron ore, which was considered as the independent solid phase. **Figure 9** shows the simulation results of the distributions of the melt fraction of the iron ore for various mass fractions of coke. Higher coke contents result in a thicker melting zone due to the higher temperature and longer residence time in the range of the sintering temperature. Changes of the melt fraction can affect the bed conditions seriously in terms of the combustion conditions and quality of the sintered ore. The melting effect should be analyzed systematically in future research.

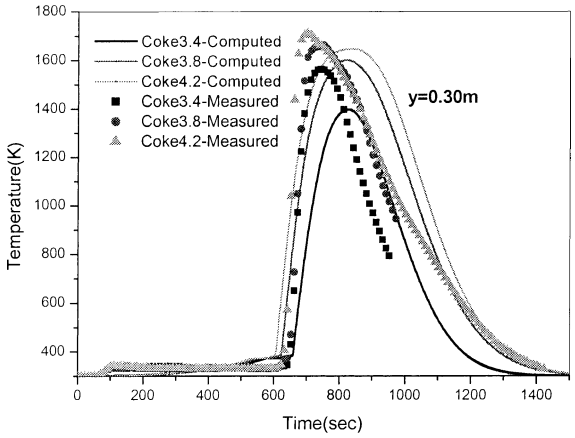

Fig. 8. Mean solid temperature at the point of $y=0.30$ m for various coke contents; simulation results and measurement results.

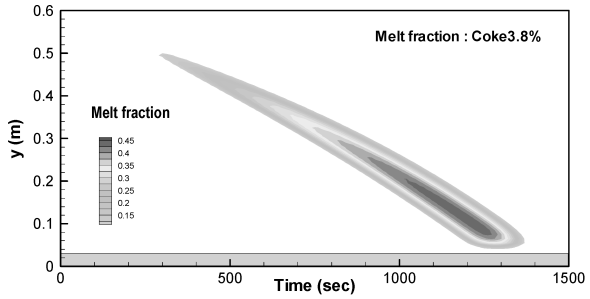

(a) Initial mass fraction of coke : 3.8%

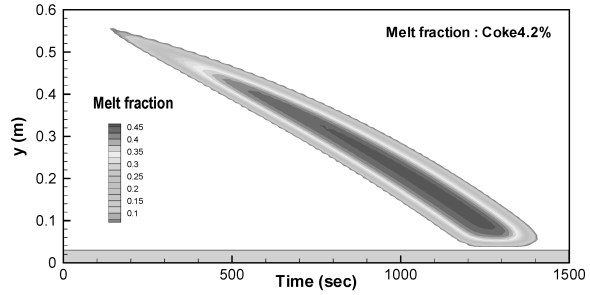

(b) Initial mass fraction of coke : 4.2%

Fig. 9. Simulation results—melt fractions of the iron ore. (a) Initial mass fraction of coke: 3.8%, (b) initial mass fraction of coke: 4.2%.

Air suction rate directly affects the coke combustion rate. A higher air suction rate causes a higher coke combustion rate. For the quantification of the simulation results, FFS (Flame Front Speed), which is defined as Eq. (24) was introduced. In this study, the numerator of Eq. (24) is defined as the distance between the location of $y=0.49$ m and that of $y=0.11$ m, where thermocouples were installed in the pot test. The 1 000 K used in Eq. (24) means the temperature at which coke combustion commences, according to the assumption in this simulation.

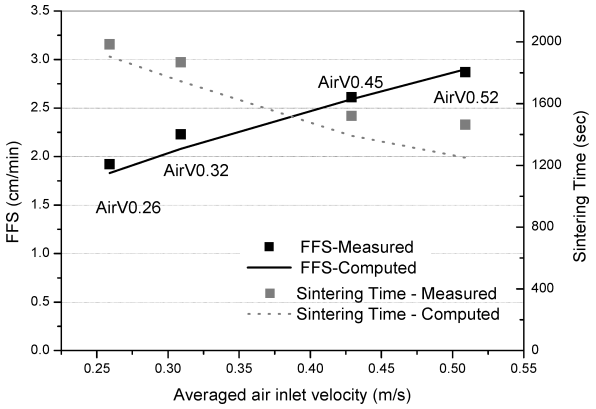

Fig. 10. FFSs' and sintering time for various inlet velocities.

$$\text{FFS (Flame Front Speed, cm/min)} = \frac{\text{Distance between two points at 1 000 K (cm)}}{\text{Time consumed for propagation (min)}} \quad ...(24)$$

Figure 10 shows the simulation and measurement results of the FFS for various air inlet velocities. It is increased proportionally to the higher initial pressure difference, causing the higher air inlet velocity. Simulation results are very close to the measurement result, meaning that the coke combustion rate can be well estimated by this numerical model.

5. Conclusion

A transient 1-dimensional model, which considers multiple solid phases, was proposed for the iron ore sintering process based on the assumption of porous media, which consist of homogeneous solid bed. Complicated modes of heat transfer in the bed were considered in detail. Modeling of radiative heat transfer and heat transfer between solid phases in the sintering bed were carried out. Bed structural changes were estimated based on the assumption that decreases in the bed height occurred due to the decrease of the particle sizes, which resulted from the surface reactions. The model also considers various kind of reactions such as drying/condensation, coke combustion and limestone decomposition. Albeit the complex nature of the phenomena, this assumption can provide reasonable values of the porosity and bed height decrease.

Calculation of this numerical model was performed for various coke contents and the air suction rates. Temperature distributions, combustion gas compositions and melt fraction distributions in the bed could be obtained. They were compared with the limited set of test results of the sintering pot. Simulation results showed a good agreement with the measured data. For improvement of the prediction, change in porosity and height of the bed influenced by surface melting should be considered in the future.

Acknowledgement

The presented work was financially supported by POSCO and was a part of the program of International Collaborative Research financially supported by Korea Ministry of Science and Technology.

REFERENCES

1) I. Muchi and J. Higuchi: *Tetsu-to-Hagané*, **56** (1970), 371.
2) R. W. Young: *Ironmaking Steelmaking*, **6** (1977), 321.
3) M. J. Cumming and J. A. Thurlby: *Ironmaking Steelmaking*, **17** (1990), 245.
4) F. Patisson, J. P. Bellot, D. Ablitzer, E. Marli, C. Dulcy and J. M. Steiler: *Ironmaking Steelmaking*, **18** (1991), 89.
5) N. K. Nath, A. J. Da Silva and N. Chakraborti: *Steel Res.*, **68** (1997), 285.
6) E. Kasai, M. V. Ramos, J. Kano, F. Saito and Y. Waseda: Proc. of 3rd World Cong. Particle Technol. (CD-ROM), ICHEME, Rugby, (1998), No. 89.
7) M. V. Ramos, E. Kasai, J. Kano and T. Nakamura: *ISIJ Int.*, **40** (2000), 448.
8) D. H. Shin and S. Choi: *Combust. Flame*, **121** (2000), 167.
9) N. Wakao and S. Kaguei: Heat and Mass Transfer in Packed Beds, Gordon and Breach Science Publishers, New York, (1982).
10) J. A. M. Kuipers, W. Prins and W. P. M. van Swaaij: *AIChE J.*, **38** (1992), 1079.
11) P. R. Austin, H. Nogami and J. Yagi: *ISIJ Int.*, **37** (1997), 458.
12) R. B. Bird, W. E. Stewart and E. N. Lightfoot: Transport Phenomena, 2nd ed., Wiley Int., New York, (2001), 525.
13) D. Merrick: *Fuel*, **62** (1983), 540.
14) R. H. Perry and D. Green: Perry's Chemical Engineers Handbook, 7th ed., McGraw-Hill, New York, (1997).